Getting the Bugs Out

Huseyin Aniktar, Dursun Baran, Enes Karav, Eren Akkaya, Y. Serdar Birecik, and Mehmet Sezgin

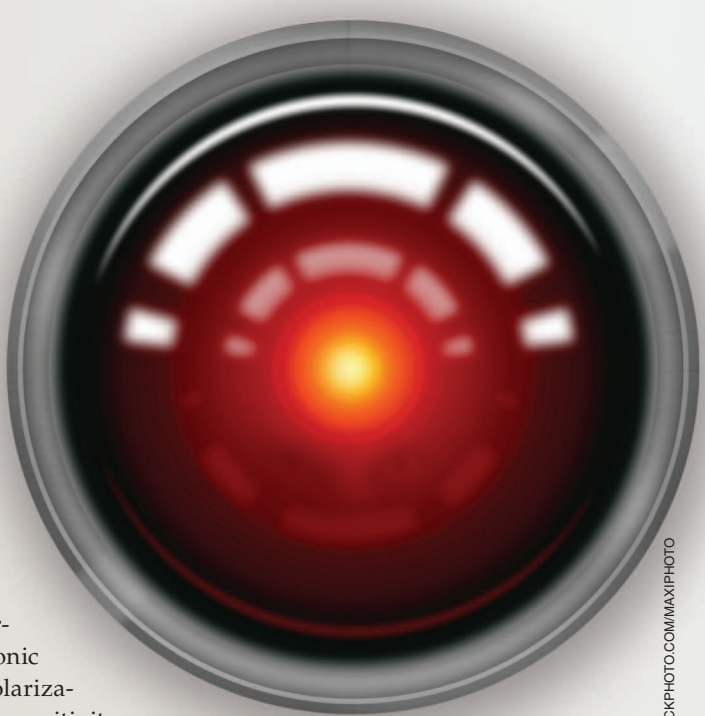

The concept of a radar that detects semiconductor and metallic objects by monitoring second and third harmonic reradiations was conceived over 35 years ago. Called *harmonic* or *nonlinear* [1], [2], these radars can transmit at one or multiple frequencies and then receive the reflected signals at, or close to, the harmonic frequencies. Recently, harmonic radars have been used in different applications such as insect and bee tracking, vital-sign monitoring, antitheft systems [3], vehicular detection and identification, and countersurveillance [4]–[7]. Important design metrics for harmonic radars include operating frequencies, waveforms, polarizations, power levels, false-alarm rates, and detection sensitivity and range [5].

For example, the authors in [8] explored the continuous wavelet transform and performed entropy analysis to improve the signal-to-noise ratio (SNR) and detection sensitivity of harmonic radars. In [9], radar transmission equations were derived using a nonlinear scattering model; here, a nonlinear junction was modeled as a nonlinear circuit network, and the formulas for calculating scattered signal characteristics were provided. False alarms are a

Huseyin Aniktar (huseyin.aniktar@tubitak.gov.tr), Dursun Baran (dursun.baran@tubitak.gov.tr), Enes Karav (enes.karav@tubitak.gov.tr), Eren Akkaya (eren.akkaya@tubitak.gov.tr), Y. Serdar Birecik (serdar.birecik@tubitak.gov.tr), and Mehmet Sezgin (mehmet.sezgin@tubitak.gov.tr) are with the Sensor and Antenna Systems Group at the Informatics and Information Security Research Center of the Scientific and Technological Research Council of Turkey, Gebze, Turkey.

Digital Object Identifier 10.1109/MMM.2015.2465591
Date of publication: 14 October 2015

major problem for harmonic radars and can be caused by system-internal harmonic leakage, corrosive or junction metals, or the presence of harmonic reflectors in the scanned area. Before the harmonic radar starts to scan the environment, it is important to be sure that the area has been sterilized of all major harmonic reflectors in range of the radar to prevent false alarms.

Harmonic Radars in Countersurveillance

Over the last decade, harmonic radars have been used for various applications in the electronic countersurveillance field. The use of a harmonic radar system has been proposed to investigate hidden electronic devices such as electronic bugs [7], [10]–[14]; this application is commonly referred to as a *nonlinear junction detector* (NLJD) [7], [10]–[15]. An NLJD allows the inspection of constructional elements in facilities, buildings, walls, and furniture to detect hidden surveillance devices such as radio microphones, tape and/or digital recorders, and other passive or active electronic devices. Such applications present an even more difficult scenario because the designer does not know the exact composition of the target.

Nonlinear Junction Detectors

In the literature, most work related to NLJDs is in the field of antenna design and optimization [16], [17]. In [12], [18], and [19], analog/digital harmonic detection techniques and their implementations for solely second harmonic are presented. In [10], the relationship between the illuminated power level and the accuracy of detection for NLJD systems is explored, and an automatic control algorithm is proposed to adapt the transmitted power. In [15], all amplification and filtering tasks are moved to the search head to prevent the self-detection that occurs when a high-transmit power signal propagates through long, flexible RF cables and RF connectors: short, rigid cables, filters, amplifiers, and antennas are integrated into a search head to increase detection sensitivity and the transmitted output power [15].

The operating principle of NLJDs is based on the nonlinearity of electronic devices [20]. All electronic devices contain P-N junctions such as diodes and transistors, all of which exhibit nonlinear behavior. These nonlinear devices reradiate the energy back to the source at double and triple the frequencies of the excitation signal. Since the basis of almost all semiconductors is the P-N junction, harmonic radar can detect almost any unshielded electronic device [7], [10]–[14]. All P-N junctions generate second and third harmonics when illuminated with sufficient RF energy, but the second harmonic is much stronger than the third harmonic for semiconductor junctions. Conversely, while corrosive or junction metals also generate harmonics [1], [21]–[23], in this case the third harmonic is stronger than the second harmonic. Sometimes these harmonics may be very close to each other, and this can cause false alarms.

Using the designed radar, a handheld system is implemented to detect hidden electronic devices.

From the mathematics of nonlinear systems, the P-N junction *V-I* (voltage-current) characteristic has an asymmetrical response, i.e., $I(V) \neq -I(-V)$ [see Figure 1(a)]. This causes strong even-order harmonics but weak odd-order harmonics. Metal–metal, or M–M, junctions or corrosives have symmetrical and noisy *V-I* responses, i.e., $I(V) \cong -I(-V)$ [see Figure 1(b)]. This causes both even and odd harmonics, but odd harmonics are closer in amplitude to even harmonics, if not even stronger. Detailed mathematical analyses can be also found in [1], [2], [8], [11], [14], [24], and [25].

A Portable Harmonic Radar for Detecting Small, Hidden Devices

In this article, we present the design and implementation of a portable harmonic radar. Harmonic radar can be implemented in two ways: either as impulse radar or as continuous wave (CW) radar. Here, we implement the harmonic radar as a stepped-frequency CW radar. This radar has a 1.95–2.05-GHz transmit capability and a 3.9–6.15-GHz receive capability, allowing the detection of up to third-order harmonics. We discuss the design tradeoffs applied to the radar and demonstrate the implemented circuits.

Using the designed radar, a handheld system is implemented to detect hidden electronic devices. The system has a +32-dBm transmitter (Tx) output power and a −130-dBm receiver (Rx) sensitivity. The implemented radar is able to detect a small semiconductor target (1.85 cm × 1.85 cm) at a distance of more than 50 cm and can accurately discriminate semiconductor targets from corrosive metals. In addition, we propose a frequency-analysis algorithm to improve the accuracy of the system further for targets that have both semiconductor and corrosive metal parts. This frequency-analysis algorithm is the most important novelty of the implemented radar: the harmonic radar's accuracy is improved by analyzing the target over a wide frequency band and interpreting the obtained results.

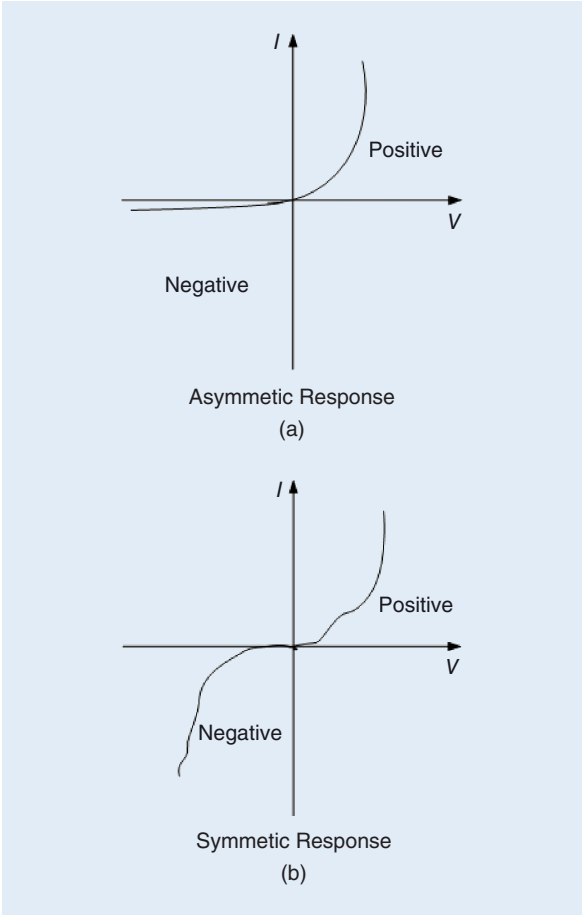

Figure 1. *(a) The P-N junction* V-I *characteristic and (b) the M–M junction* V-I *characteristic.*

We also show designs we have implemented for special Tx and Rx antennas and discuss important specifications to reduce the internal system leakages of harmonics and so improve system accuracy.

System-Level Considerations

Detection Range and Accuracy

The issues most commonly encountered with NLJD systems are detection range and accuracy [10]–[12], [18]. Detection range depends on the target objects and the system's sensitivity. Some target objects reflect strong signals, and some reflect weak signals when they are illuminated by electromagnetic energy. The reflected signal depends on the target object's internal structure (which consists of many diodes, transistors, bond-wire lengths, and shapes), its angle, and the electromagnetic characteristics of the environment. Since the system user cannot know the target objects, it is possible to make the system more sensitive by optimizing the circuit- and system-related design parameters to increase the detection range.

Accuracy deteriorates as a result of system-related leakage as well as target-related characteristics. Received harmonic-level comparison includes some uncontrolled parameters coming from the target. These uncontrolled target parameters can be objects that have different behaviors (e.g., RF filtering and amplification) at the second and the third harmonic frequencies. In addition, the signal path loss will be quite different for the harmonics: because of its lower frequency, the second harmonic has a lower path loss compared to the third harmonic. Moreover, the path loss depends on the working environment. Therefore, some correction strategy must be developed to improve system accuracy.

Technical Details

Before discussing the system's implementation, we need to consider some technical details about the system's operation, based on the assumption that the system has a flat, even response over all possible operating conditions and frequency ranges. Think of a P-N junction in an integrated circuit (IC), and imagine that this P-N junction is connected to a bond wire, an external pin, and printed circuit board (PCB) tracks that behave as an antenna for the radiation. When this IC is illuminated with sufficient RF energy, the amount of power reaching the target P-N junction, P_R, is

$$P_R = G_T.G_{TO-FF}.G_{P-FF}.P_t \quad [W], \tag{1}$$

where G_T is the Tx antenna gain of the system, G_{TO-FF} is the reception gain of P-N junction at the fundamental frequency, G_{P-FF} is the path loss at the fundamental frequency, and P_t is the transmitted output power of the system.

The P-N junction will generate second and third harmonics from the energy in the received signal. The measured harmonic signals are calculated in (2) and (3) as

$$P_{H\,R2} = P_R.CG_{H\,R2}.G_{TO-H\,R2}.G_{P-H\,R2}.G_R \quad [W] \tag{2}$$

$$P_{H\,R3} = P_R.\,CG_{H\,R3}.\,G_{TO-H\,R3}.\,G_{P-H\,R3}.\,G_R \quad [W], \tag{3}$$

where $P_{H\,R2}$ and $P_{H\,R3}$ are the second and third harmonic powers measured by the radar Rx, $CG_{H\,R2}$ and $CG_{H\,R3}$ are the conversion gain at the second and third harmonic frequencies, $G_{TO-H\,R2}$ and $G_{TO-H\,R3}$ are the transmit gain of the P-N junction at the second and third harmonic frequencies, $G_{P-H\,R2}$ and $G_{P-H\,R3}$ are the path losses at the second and third harmonic frequencies, and G_R is the Rx antenna gain of system.

Using (2) and (3), the power ratio of the measured harmonics is calculated as

$$\frac{P_{H\,R2}}{P_{H\,R3}} = \frac{P_R.\,CG_{H\,R2}.\,G_{TO-H\,R2}.\,G_{P-H\,R2}.\,G_R}{P_R.\,CG_{H\,R3}.\,G_{TO-H\,R3}.\,G_{P-H\,R3}.\,G_R} = \frac{CG_{H\,R2}.\,G_{TO-H\,R2}.\,G_{P-H\,R2}}{CG_{H\,R3}.\,G_{TO-H\,R3}.\,G_{P-H\,R3}} \tag{4}$$

$$\log\left(\frac{P_{H\,R2}}{P_{H\,R3}}\right) = \log\left(\frac{CG_{H\,R2}}{CG_{H\,R3}}\right) + \log\left(\frac{G_{TO-H\,R2}}{G_{TO-H\,R3}}\right) + \log\left(\frac{G_{P-H\,R2}}{G_{P-H\,R3}}\right) \tag{5}$$

$$\log\left(\frac{CG_{H\,R2}}{CG_{H\,R3}}\right) = \log\left(\frac{P_{H\,R2}}{P_{H\,R3}}\right) - \log\left(\frac{G_{TO-H\,R2}}{G_{TO-H\,R3}}\right) - \log\left(\frac{G_{P-H\,R2}}{G_{P-H\,R3}}\right) \quad (6)$$

$$\log\left(\frac{CG_{H\,R2}}{CG_{H\,R3}}\right) = \log\left(\frac{P_{H\,R2}}{P_{H\,R3}}\right) - CF. \quad (7)$$

To make a true comparison, it is necessary to use the conversion gains for the second and the third harmonics because these represent the target's actual response to the received power. As seen in (4)–(7), directly comparing the measured harmonic signals does not provide a correct result. However, neither is it possible to directly measure the conversion gains. The measured harmonic magnitudes must be updated with a correction factor as given in (7). The correction factor is composed of two elements: the first stands for the difference of the target object's behavior at the harmonic frequencies; the second stands for the path-loss difference. As the preceding analysis suggests, the correction factor depends on the target object *and* the path loss.

In addition, it is clear that the correction factor is frequency dependent and, as a consequence, difficult to calculate mathematically. Therefore, a good approach is to operate the system at multiple transmit frequencies to reduce the false alarms. For the simplest scenario, if the line-of-sight condition is assumed and the Friis equation [26] is used, the path loss difference can be calculated using the formula

$$\log\left(\frac{G_{P-HR2}}{G_{P-HR3}}\right) = \log\left(\frac{\lambda_{HR2}^2}{\lambda_{HR3}^2}\right), \quad (8)$$

where $\lambda_{H\,R2}(\lambda_{H\,R3})$ is the signal wavelength at the second (third) harmonic frequency. The path loss difference between the second and third harmonics becomes 3.52 dB when the fundamental frequency is 2 GHz. The second and third harmonics, HR2 and HR3, are at 4 GHz and 6 GHz, respectively.

Study Specifics

For our work, we selected concrete as an example of a tough working environment because of its high signal attenuation. Another important environmental characteristic is the level of wetness. Wet working environments (such as concrete or insufficiently dried wood) cause even harsher RF signal attenuation. In [27], the authors provide detailed path-loss analyses for different environmental conditions, e.g., glass, lumber, plywood, plain concrete, and brick.

We measured the path losses for the air and the concrete (C35 class) at different distances using an experimental setup. In this setup, both the Rx and the Tx antennas were located on opposite sides of the material target (one side being air, the other side concrete), with the signal generator powered up to +0 dBm. The Rx antenna was connected to a spectrum analyzer, and the received signal was measured. This experiment was performed for different thicknesses of concrete and different stand-off distances.

The measured values are provided in Table 1. There could be a ±1-dB measurement error because of the cable, the connector loss estimation, reading errors, and the measurement system's accuracy and calibration. As these results show, the working environment has a direct role in the path-loss ratio and can reach 25.3 dB for a 30-cm plain concrete wall [27].

Portable Harmonic Radar System Components and Implementation

Figure 2 shows the block diagram of the harmonic radar system, which consists of Tx and Rx antennas, an RF/microwave circuit with optimized system specifications (a highly sensitive Rx, high transmission power with low power consumption, etc.), a digitizer, and a central processing unit to run the application and the graphical user interface (GUI). An important design challenge for this type of harmonic radar is the

TABLE 1. Path loss measurements for air and the concrete.

Frequency	Air (30 cm)	Air (15 cm)	Concrete (30 cm)	Concrete (15 cm)
2 GHz	29.2 ±1 dB	22.5 ±1 dB	55.8 ± 1 dB	31.8 ±1 dB
4 GHz	33.8 ±1 dB	27.8 ±1 dB	91.7 ± 1 dB	46.9 ±1 dB
6 GHz	36.9 ±1 dB	31.1 ±1 dB	117.0 ± 1 dB	63.7 ±1 dB
Path loss difference	3.1 dB	3.3 dB	25.3 dB	16.8 dB

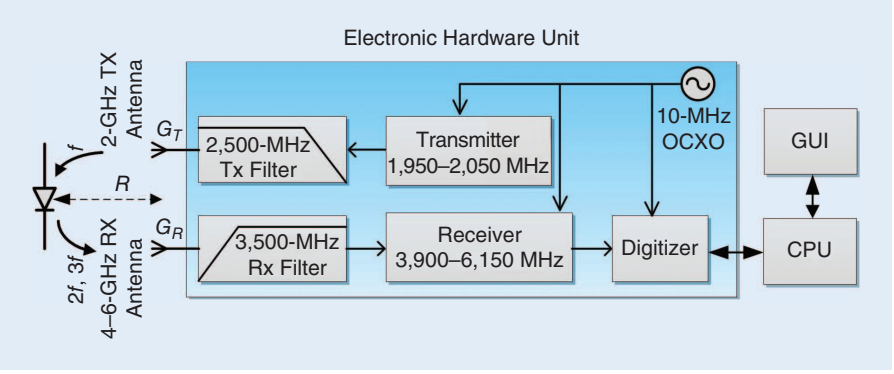

Figure 2. *The block diagram of the implemented harmonic radar system. GUI: graphical user interface; CPU: central processing unit.*

isolation of the Tx from the Rx. Recent moves toward higher transmitted output power and a more sensitive Rx make the problem even harder.

Instead of using a circulator or diplexer at the Tx/Rx terminal for a single antenna, the Tx and the Rx are physically separated, which increases the harmonic isolation between these two sides. This reduces false alarms resulting from any internal harmonics generated by the Tx circuit, so the system will be sensitive only to harmonics reflected by target objects. With the single-antenna option using a diplexer or a circulator, high isolation is achieved by the Tx and Rx filters, which, consequently, need to be quite sharp. Physical separation of the Tx and Rx relaxes the specifications for the Tx and Rx filter.

In the system, a high-quality 10-MHz oven-controlled crystal oscillator (OCXO) is used to synchronize the Tx, the Rx, and the digitizer. Synchronization is important when the digitizer results are used to measure harmonic strengths. The operating frequency for the Tx is selected at between 1,950 and 2,050 MHz; the selected Rx frequency range is between 3,900 and 4,100 MHz for the second harmonic and between 5,850 and 6,150 MHz for the third harmonic. The Rx is able to detect between 3,900 and 6,150 MHz, and it is time-multiplexed to get the second and the third harmonics (the Rx is tuned to the second and third harmonic in turn). The choice of operating frequencies depends on the target size resolution and the detection distance. Using high frequencies, such as 2 GHz, allows small objects to be detected, but only at short detection distances. Using lower operating frequencies, such as 900 MHz, allows targets to be detected at longer distances, but the system is more sensitive to relatively larger objects [26].

Harmonic Radar Tx

The design specifications for the Tx of the harmonic radar system are high-output RF power (greater than 30 dBm), low frequency settling error (less than 50 kHz), fast frequency settling time (fewer than 3 ms), suppressed harmonics (80 dB lower than fundamental frequency), and low power dissipation. A wideband frequency synthesizer (model LTC6946-2 from Linear Technology) is used to generate a transmit signal in the range of 1,950–2,050 MHz with an approximate 0 dBm output RF power. The transmit signal is low-pass filtered to eliminate harmonics and then preamplified with a linear amplifier (model RFLA1018DS from RFMD) with a 25-dB gain. The transmit signal is again low-pass filtered and then power amplified (model HMC453QS16 from Hittite) in the last stage.

The obtained output power from the Tx is approximately +32 dBm, and the antenna gain is added to this value to get the effective radiated RF power. Total power dissipation of the Tx is about 6 W. The block diagram of the TX is illustrated in Figure 3(a). The frequency settling time is around 1.5 ms, and the frequency settling error is around 30 kHz. The

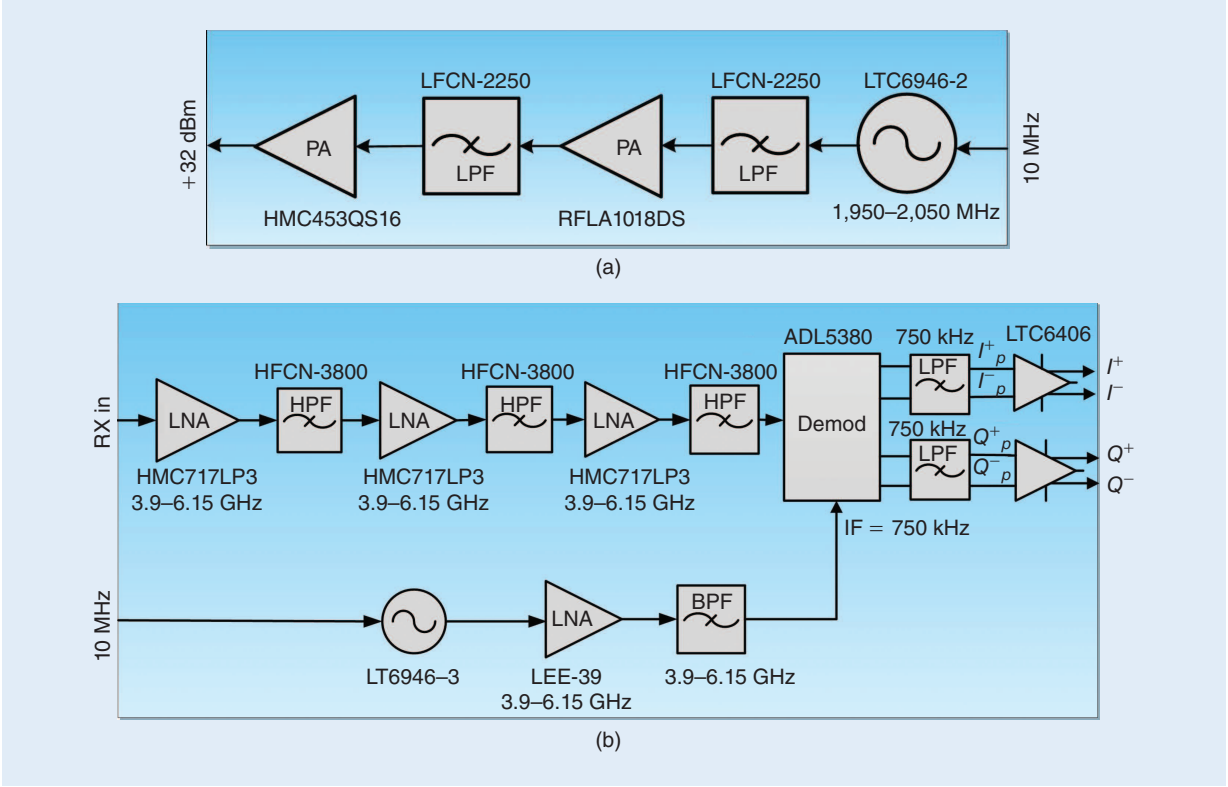

Figure 3. *Block diagrams for (a) the harmonic radar Tx and (b) the harmonic radar Rx. PA: power amplifier; LPF: low-pass filter; LNA: low-noise amplifier; HPF: high-pass filter; demod: demodulator; BPF: bandpass filter.*

Tx is controlled using an serial peripheral interface provided from the controller's field-programmable gate array (FPGA) core. In addition, digital output power control functionality is implemented to adjust the transmitted RF power. The size of the Tx circuit is 60 mm × 40 mm.

Harmonic Radar Rx

The harmonic radar Rx is implemented using a homodyne Rx topology. The received RF signal is amplified and filtered three times and then applied to an in-phase quadrature (IQ) demodulator that gives I and Q output signals at a 750-kHz intermediate frequency (IF). The IF signals are in differential form and are low-pass filtered and then amplified with a programmable IF amplifier. The amplified IQ outputs are fed to the digitizer. The digital side I and Q signals are fed to the real and imaginary inputs of the complex fast Fourier transform (FFT) operation. Using a single I or Q signal is also possible, at the expense of 3-dB loss on the signal level. The detailed block diagram of the Rx is illustrated in Figure 3(b).

The received signal is amplified with a low-noise amplifier that has a 1.3-dB noise figure and a 16-dB gain (model HMC717LP3 from Hittite). The received signal includes unwanted frequency components at the Tx frequency, which can generate false second and third harmonics by the Rx circuit. Therefore, a 3.8-GHz high-pass filter (model HFCN 3800 from Mini-Circuits) is applied after each low-noise amplifier at the Rx to minimize the transmitted signal flow to the Rx.

The operating frequency range of the Rx is quite large to cover the second and the third harmonics. o cover the complete Rx frequency range (3.9–6.15 GHz), a different form of frequency synthesizer (model LTC6946-3 from Linear Technology) is used in the Rx. The Tx, Rx, and digitizer are fed with the same 10-MHz reference oscillator for a coherent operation. The down conversion is fulfilled with a broadband IQ demodulator (model ADL5380 from Analog Devices).

The performance metrics of the Rx are summarized in Table 2. The size of the Rx circuit is 125 mm × 37 mm. In addition to analog techniques, signal bandwidth is narrowed by applying digital filters to reach the Rx sensitivity performance levels stated in Table 2.

TABLE 2. Rx performance specifications.

Rx Performance	Value
Frequency range	3,900–6,150 MHz
Input P1dB	–30 dBm
Gain	45 dB
Minimum sensitivity	–130 dBm
Noise figure	1.6 dB
Power consumption	2 W
IF	750 kHz

Tx and Rx Filters

The ideal Tx filter is supposed to reduce the level of harmonics generated by the Tx circuit to the Tx antenna, while the transmitted signal can pass without loss. The Tx filter is a low-pass filter, and the filter passband is dc to 2.5 GHz with a maximum insertion loss of 1 dB. The filter passband voltage standing wave ratio (VSWR) is about 1.9:1. Filter stopband rejections are about 75 dB at 4 GHz and 68 dB at 6 GHz. The Tx filter is implemented on a PCB with two surface-mount low-pass filters (model LFCN-2600 from Mini-Circuits) cascaded on RO4003 laminate material manufactured by Rodgers. The size of the Tx filter circuit is 35 mm × 15 mm.

The Rx filter is used to reduce the level of the transmitted signal to the Rx. The Rx filter is implemented as a high-pass filter. The filter passband is around 3.5 GHz to 10 GHz, with a maximum insertion loss of 1 dB. The

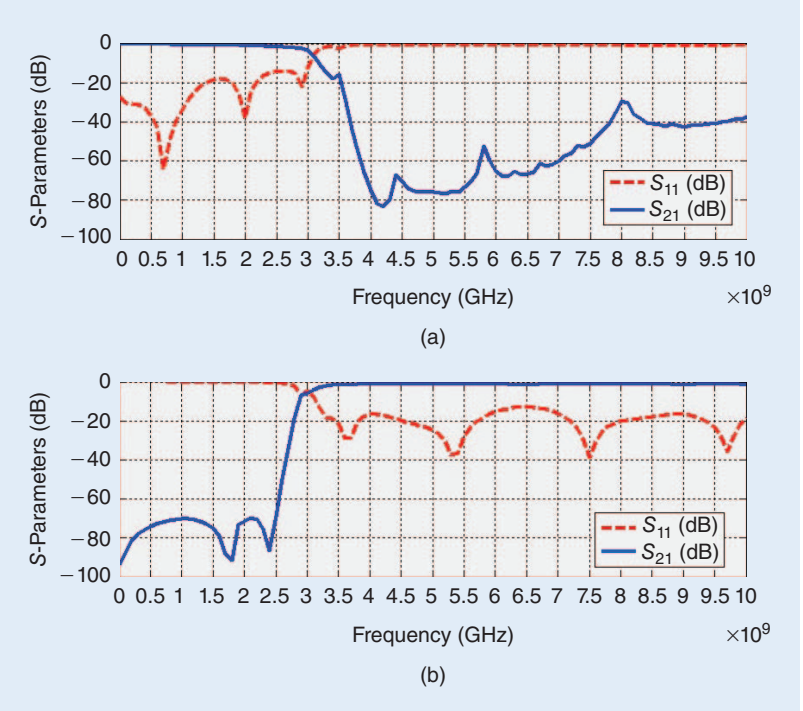

Figure 4. *S-parameter characteristics for (a) the Tx low-pass filter and (b) the Rx high-pass filter.*

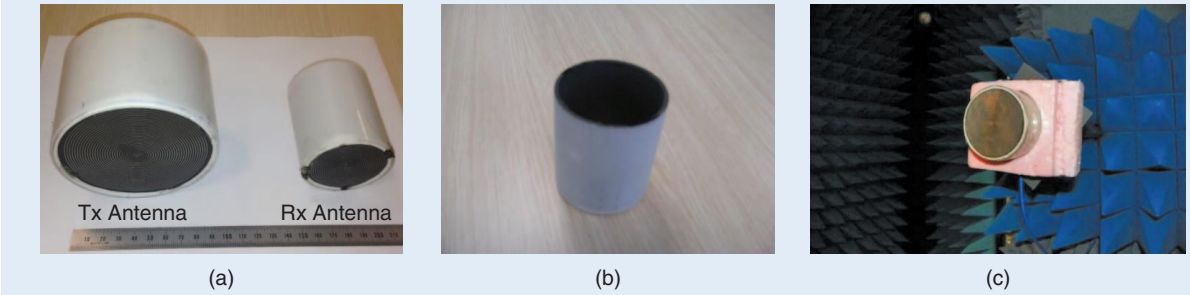

Figure 5. *(a) The Tx and Rx antennas. (b) The nickel spray-coated metallization layer. (c) The antenna measurement setup in an anechoic chamber.*

filter passband VSWR is about 1.7:1. The filter stopband rejection is about 76 dB at 2 GHz. The Rx filter is implemented on a PCB with two surface-mount high-pass filters (model HFCN-3100 from Mini-Circuits) cascaded on the RO4003 material. The size of the Rx filter circuit is 34 mm × 16 mm.

Both the Rx and Tx filters were measured by a vector network analyzer. Figure 4 illustrates the S-parameter characteristics for the Tx and Rx filters.

Tx and Rx Antennas

With NLJD applications, it is impossible to determine the Tx and the Rx antenna polarizations without knowing the target and its position/orientation. Under linear polarization transmitting conditions, the orientation of the target has a direct effect on the signal power delivered to the target. Therefore, a circularly polarized antenna with a perfect axial ratio was chosen to eliminate the risk of not delivering enough power to the target. As a result, a spiral antenna type was chosen and implemented [16], [17], [28]. The axial ratio is the ratio of the major axis to the minor axis of the polarization ellipse and should be less than 3 dB for circular polarization. An axial ratio of 0 dB means a pure circularly polarized antenna.

The Tx antenna is a 2-GHz left-hand circularly polarized spiral antenna as shown in Figure 5(a). The antenna gain is measured as −0.6 dBi, and the axial ratio is 1.1 dB. The S_{11} of the antenna is measured as −14.5 dB. The antenna's diameter is 10 cm, and its height is 7 cm. To reduce backside radiation of the antenna, an Eccosorb AN-75 series multilayer absorber is used in the antenna's back cavity. The antenna's backside radiation should be as low as possible to avoid any potential interference and any parasitic, and thus false, alarms. The Tx antenna measurement setup and the radiation pattern measurement are illustrated in Figure 5(c) and Figure 6(a), respectively.

The Rx antenna is a 4–6-GHz left-hand circularly polarized spiral antenna as shown in Figure 5(a). The antenna gain is measured as 2.4 dBi and 3.14 dBi at 4 GHz and 6 GHz, respectively. The axial ratio is measured as 0.7 dB and 0.5 dB at 4 GHz and 6 GHz,

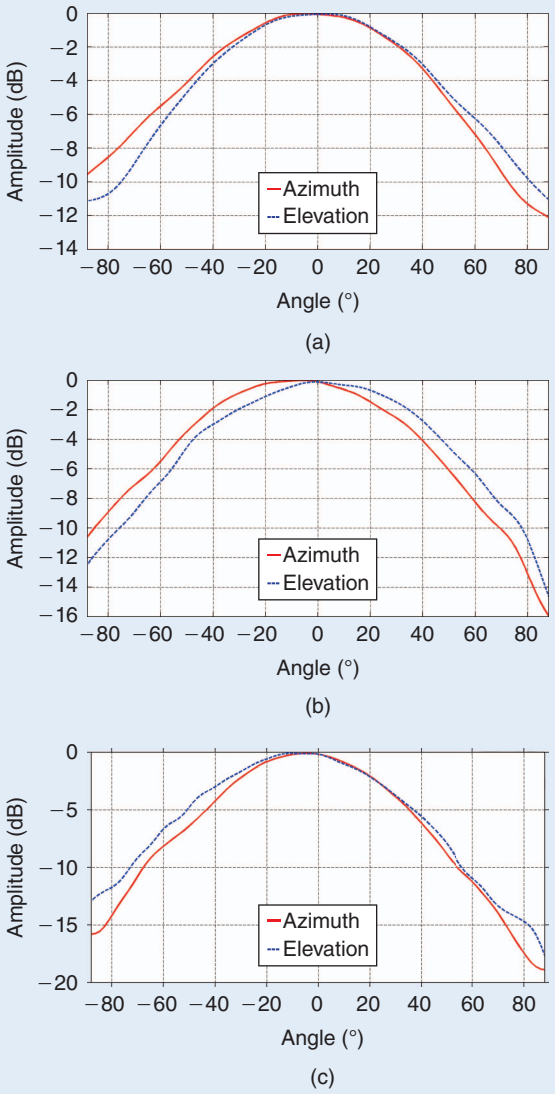

Figure 6. *The radiation pattern measurements for the Tx and Rx antennas: (a) the 2-GHz spiral antenna radiation pattern for the Tx, (b) the 4-GHz spiral antenna radiation pattern for the Rx, and (c) the 6-GHz spiral antenna radiation pattern for the Rx.*

respectively. The S_{11} of the antenna is below −13.5 dB through the 4–6 GHz frequency bands. The antenna's diameter is 6 cm, and its height is 7 cm. The Rx antenna is designed at 2 GHz to reduce coupling the level between the Tx and Rx antennas at the transmitting frequency. The antenna gain is measured as −14.5 dBi at 2 GHz. To reduce backside radiation of the antenna, an Eccosorb AN-74 series multilayer absorber is used in the antenna back cavity. The Rx antenna measurement setup and the radiation pattern measurements are illustrated in Figure 5(c) and Figure 6(b) and 6(c), respectively.

The Tx and Rx antenna polarizations are the same because the reflected signal, which strongly reflects from the wall face, is cross-polarized, so another coupling reduction advantage is gained at the Rx side.

The impedance matching of the Tx and Rx spiral antennas is achieved by incorporating a broadband balun into the feeding structure. The isolation between the Tx and Rx antennas is measured as 48 dB at 2 GHz, 57 dB at 4 GHz, and 59 dB at 6 GHz.

The spiral antenna needs to be backed with a closed metallic cavity to a radiate a unidirectional beam to enhance the antenna gain and the radiation efficiency. The drawback of using this cavity is observed on the circular polarization behavior through the whole frequency band due to multiple reflections from the cavity wall. The closed metallic cavity is filled with an absorber to overcome this problem, with gain degradation, on the other hand, enhancing the circular polarization characteristics of the antenna in the desired frequency range. The cavity is implemented as a plastic (Delrin) cover with nickel spray coating (ENSCP 400H) from Electrolube instead of a heavy mechanical material [see Figure 5(b)]. Using nickel spray coating as a metallization layer for the cavity reduces the Tx and Rx antenna weights significantly and, therefore, total system weight, but at the expense of a slight reduction in the antenna gains.

The total Tx antenna weight is 124 g, and the total Rx antenna weight is 62 g. In total, the plastic cover implementation provides 38% lighter antennas as compared to an aluminum cover implementation. Such light implementation is critical for portable systems.

Digitizer

The digitizer is the third main block of the electronic hardware unit. Its task is to convert the analog signals coming from the I and Q paths on the Rx channels. Therefore, two analog-to-digital converter (ADC) channels are required, and they must be synchronized. A critical issue with this block is the implementation of a phase-synchronized design between the ADC channels. To alleviate this design constraint, a quad 14-bit ADC chip with a single encode clock (model LTC-2171 from Linear Technology) is utilized.

The issues most commonly encountered with NLJD systems are detection range and accuracy.

The encode clock is fed to the internal phased-lock loop block to generate the sampling signal and is distributed to all ADC cores within the same IC. The encode clock is fed from the common 10-MHz reference clock.

The digitized outputs are in serial low-voltage differential signaling (LVDS) format, and deserialization is implemented by the FPGA core. The serial LVDS output format is used to reduce the pin count needed to capture ADC data by the FPGA core. The total power dissipation of the digitizer is about 3 W. The size of the digitizer circuit is 110 mm × 70 mm.

A 10-MHz sampling clock is used to collect 8-k samples, and 8k-FFT results are calculated. Rectangular windowing is used. These operations are repeated eight times, and the results are summed to obtain an average over all the measurements. This process is repeated for the second and the third harmonic frequencies. The whole process is completed within 22.24 ms with a 100-MHz FPGA clock.

Analysis Algorithm and Experimental Results

The system described was implemented and applied to several test objects. Different types of semiconductor targets (labeled ST) are used to test the system. An RF mixer (ST_1, 1.85 cm × 1.85 cm), an IC circuit (ST_3, 1.85 cm × 1.85 cm), and an active RFID Tx (ST_4, 2.5-cm diameter) were chosen and are shown in Figure 7(a). In addition, a

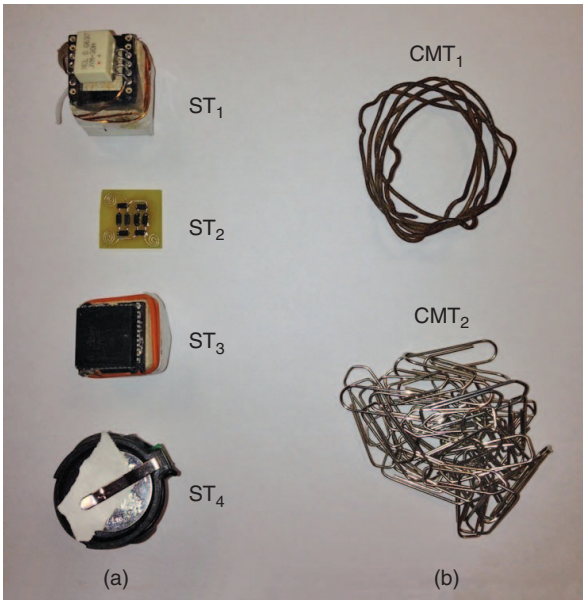

Figure 7. *The test objects used in the experiments: (a) the semiconductor targets and (b) the corrosive metal targets.*

semiconductor target was designed with several diodes (an RF mixer topology) and implemented on a PCB (ST_2, 1.85 cm × 1.85 cm), also shown in Figure 7(a).

To simulate the false alarm condition, two corrosive metal targets (labeled CMT) were constructed (CMT_1 with construction wire, 5-cm diameter, and CMT_2 with paper clips, 5-cm diameter), as shown in Figure 7(b). When two metals are touching each other, a false alarm may be generated by a nonlinear junction between these metals since M–M junctions also generate harmonics. The system may interpret this object as a semiconductor by only looking at the received harmonic levels. Ideally, this object should be detected as an M–M junction. However, the effects explained earlier cause the system to interpret this target as a semiconductor object. When the system detects a semiconductor, the second harmonic will be greater than the third harmonic; for the corrosive metal detection, the scenario will be reversed. To compare the results quantitatively, a measure called the certainty measure (CM) is defined and calculated as

$$\mathrm{CM}_2 = \frac{P_{H\,R2}}{P_{H\,R3}} \tag{9}$$

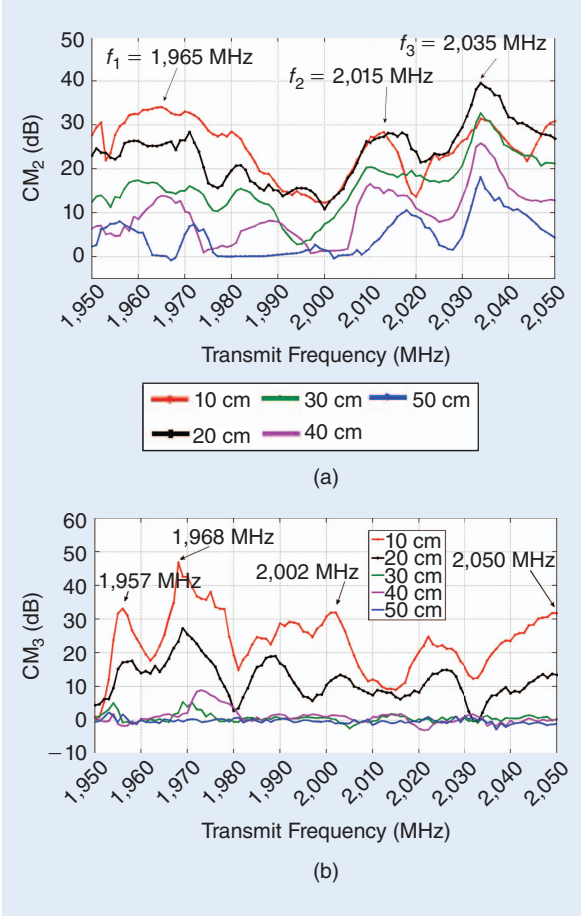

Figure 8. *CMs for selected targets: (a) the second harmonic certainty measure (CM_2) for ST_2 and (b) the third harmonic certainty measure (CM_3) for CMT_1.*

$$\mathrm{CM}_3 = \frac{P_{H\,R3}}{P_{H\,R2}}, \tag{10}$$

where $P_{H\,R2}$ is the second harmonic power level and $P_{H\,R3}$ is the third harmonic power level.

Note that the measured harmonic levels should be corrected with the correction factor as given in (7). In (9) and (10), the correction factor is ignored because it is not possible to calculate it exactly. Instead of exactly calculating the correction factor, it is possible to observe its effect by running some experiments on the target. The correction factor depends on the target harmonic characteristics and the path-loss difference at the harmonic frequencies. At each transmit frequency, the correction factor can be changed by varying the path-loss difference as one moves closer to or further from the target. However, this technique does not ensure that the correction factor gets close to zero since the path loss at the third harmonic frequency is always larger than that at the second harmonic frequency. To generate the possible scenarios for the correction factor to approach zero, this process is repeated at different transmit frequencies.

After completing the process, it is possible to draw the following conclusions. Increasing the distance improves the semiconductor detection probability at a given transmit frequency, and similarly reducing the distance improves the corrosive metal detection possibility. In addition to the distance, some transmit frequencies are good for semiconductor detection, and some are good for corrosive metal detection. Therefore, by sweeping the distance and the transmit frequency, more target scenarios are measured, and the obtained results have an improved probability of containing the scenarios at which the correction factor is sufficiently small to make the correct decision.

The measured results when the target objects are placed at 10 cm, 20 cm, 30 cm, 40 cm, and 50 cm away from the sensor head are given in Figure 8(a) for ST_2 and Figure 8(b) for CMT_1. This process is repeated for the Tx frequency range of 1,950 MHz–2,050 MHz. The Tx, the Rx, and the Tx and Rx antennas are assumed to have equal characteristics in this frequency range since the maximum antenna gain fluctuation is less than 1 dB in the transmitted RF power, the Rx sensitivity, and the antenna gain. The test environment is also clean of any interference, i.e., there should not be any signal on the Rx spectrum above −130 dBm when the Tx is off.

As shown in Figure 8(a) and (b), some frequencies provide higher detection sensitivity depending on the characteristics of the target objects and the distance. The frequencies close to 1,965 MHz, 2,015 MHz, and 2,035 MHz are good for detection of the semiconductor (ST_2), and those close to 1,957 MHz, 1,968 MHz, 2,002 MHz, and 2,050 MHz are good for detection of the corrosive metal target (CMT_1). Some frequencies can

activate the P-N junction of the target better than other frequencies, which the results illustrate. These results will be different when different targets are used. Therefore, there is no best operating frequency for all targets. The Tx must be swept over the entire operating frequency range to increase the detection sensitivity and the accuracy of the harmonic radar. These figures show that transmitting on multiple frequencies and evaluating results in a logical way can provide better accuracy and sensitivity.

When the target object is composed of purely semiconductor material or purely of corrosive metal, the system can more accurately make the correct detection because the received harmonic signals have good SNR values to reach a conclusion. However, when the semiconductor material and the corrosive metals are both in the target, the system will generate many signals of close harmonic strength, and it is hard to come up with a conclusion. Figure 9 represents the scenario when a semiconductor object (ST_3) and a corrosive metal object (CMT_1) are found together.

This is the case for most current electronic bugs since they include both semiconductor material and corrosive metals. An example of a corrosive metal is the antenna part of an electronic bug. Most current NLJD systems try to come up with single result: either a semiconductor or a corrosive metal [7], [10], [11]. However, this limits the user's knowledge about the target and may result in false conclusions. Instead of making a single estimate, the percentage of the likelihood for a target being 1) a semiconductor, 2) a corrosive metal, 3) undetermined, or 4) not detected, respectively, can be provided over the transmit frequency range to increase the user's interpretative ability. In the remainder of this section, we will discuss he detection algorithm for accomplishing this likelihood (illustrated in Figure 10).

Each object has a different composition of semiconductor and corrosive parts. Therefore, we expect to see a signature for each target at the results of the algorithm. When the distance is incorporated into the result, the following experimental conclusions can be made. For purely semiconductor targets, the semiconductor detection percentage is expected to be high, and there may be a small percentage of undetermined or corrosive metal detection cases at a short distance. We assume a "short distance" to be 10 cm for purposes of our work, but it could be any possible value.

As the distance is increased, the corrosive metal and undetermined percentages move toward the semiconductor percentage. For purely corrosive metal targets, the corrosive metal or undetermined percentage is expected to be high, and the semiconductor percentage low at a short distance. As the distance is increased, the semiconductor percentages move toward the corrosive metal or undetermined percentages. For a mix of semiconductor material and corrosive metal, both the corrosive metal and semiconductor percentages are expected to be high at a short distance.

The choice of operating frequencies depends on the target size resolution and the detection distance.

Figure 9. *A target consisting of both semiconductor material and corrosive metal.*

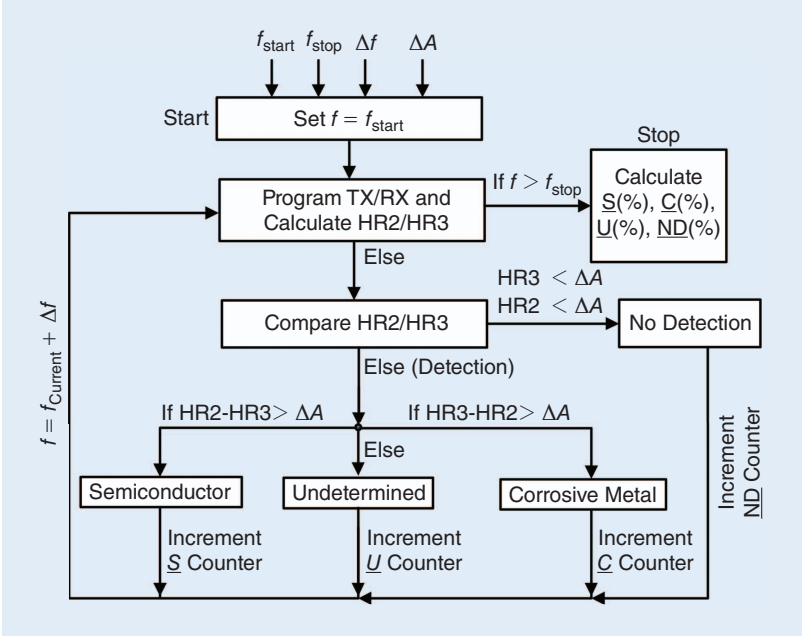

Figure 10. *A proposed algorithm for frequency response analysis and detection. S: semiconductor; C: corrosive metal; U: undetermined; ND: not detected.*

We propose a frequency-analysis algorithm to improve the accuracy of the system for targets that have both semiconductor and corrosive metal parts.

The semiconductor part is detected at the transmit frequencies where the semiconductor detection sensitivity is higher. The corrosive metal part is detected at the frequencies where the corrosive metal detection sensitivity is higher. As the distance is increased, the semiconductor percentage will become larger, and the corrosive metal/undetermined percentage will grow smaller. After a certain distance, all results will convert to not detected, depending on the target. These experimental conclusions can be extended as more targets are applied to the test. The algorithm tries to increase the user's interpretative ability to explore the target's characteristics.

As noted previously, targets are classified into four groups: semiconductor, corrosive metal, undetermined, and not detected. When the second and the third harmonic amplitudes are lower than some threshold level (in our work, we define this as SNR = 5 dB), the target is classified as not detected. When the received harmonic amplitudes are greater than the threshold level and close to each other, the system cannot reach a conclusion, and the target is classified as undetermined. When some of the received harmonic amplitudes are greater than the threshold level and the second harmonic is larger than the third harmonic above a certain level ($\Delta A = P_{H\,R2} - P_{H\,R3} \geq 5$ dB), the target is classified as semiconductor. When some of the received harmonics are greater than threshold level and the third harmonic is larger than the second harmonic above a certain level ($\Delta A = P_{H\,R3} - P_{H\,R2} \geq 5$ dB), the target is classified as corrosive metal. This classification is repeated over a range of transmit frequencies.

Operating on multiple transmit frequencies can increase the system's accuracy. The novel detection algorithm we have developed (Figure 10) provides a percentage measure for the likelihood of a target being semiconductor, corrosive metal, undetermined, or not detected. The transmit frequency is swept from a start point to a stop point, and each run is classified to obtain a percentage. The system's user will be able made a conclusion based on the likelihood of possible cases.

TABLE 3. Frequency response analysis for the test objects: example 1.

f_{start} = 1,950 MHz, f_{stop} = 2,050 MHz, Δf = 1 MHz, ΔA = 10 dB

S (%), C (%), U (%), ND (%)

	10 cm	30 cm	50 cm
ST_1	61, 0, 39, 0	99, 0, 1, 0	100, 0, 0, 0
ST_2	100, 0, 0, 0	85, 0, 1, 14	11, 0, 0, 89
ST_3	85, 0, 15, 0	100, 0, 0, 0	100, 0, 0, 0
ST_4	100, 0, 0, 0	100, 0, 0, 0	85, 0, 3, 12
CMT_1	0, 98, 2, 0	0, 0, 5, 95	0, 0, 0, 100
CMT_2	0, 95, 5, 0	1, 78, 19, 2	0, 33, 27, 40
Both	24, 5, 70, 0	46, 0, 54, 0	98, 0, 2, 0

TABLE 4. Frequency response analysis for the test objects: example 2.

f_{start} = 1,950 MHz, f_{stop} = 2,050 MHz, Δf = 10 MHz, ΔA = 10 dB

S (%), C (%), U (%), ND (%)

	10 cm	30 cm	50 cm
ST_1	55, 0, 45, 0	100, 0, 0, 0	100, 0, 0, 0
ST_2	100, 0, 0, 0	89, 0, 2, 9	9, 0, 0, 91
ST_3	82, 0, 18, 0	100, 0, 0, 0	100, 0, 0, 0
ST_4	100, 0, 0, 0	100, 0, 0, 0	91, 0, 0, 9
CMT_1	0, 100, 0, 0	0, 0, 10, 90	0, 0, 0, 100
CMT_2	0, 100, 0, 0	0, 73, 18, 9	0, 28, 27, 45
Both	27, 9, 64, 0	36, 0, 64, 0	91, 0, 9, 0

TABLE 5. Frequency response analysis for the test objects: example 3.

f_{start} = 1,950 MHz, f_{stop} = 2,050 MHz, Δf = 1 MHz, ΔA = 5 dB

S (%), C (%), U (%), ND (%)

	10 cm	30 cm	50 cm
ST_1	94, 0 , 6, 0	100, 0, 0, 0	100, 0, 0, 0
ST_2	100, 0, 0, 0	95, 0, 1, 4	55, 0, 8, 37
ST_3	93, 0, 7, 0	100, 0, 0, 0	100, 0, 0, 0
ST_4	100, 0, 0, 0	100, 0, 0, 0	93, 0, 3, 4
CMT_1	0, 99, 1, 0	0, 5, 4, 91	0, 0, 0, 100
CMT_2	0, 98, 2, 0	2, 88, 10, 0	0, 59, 19, 22
Both	44, 22, 34, 0	78, 2, 20, 0	100, 0, 0, 0

Figure 11. *(a) The normal operational mode and (b) the analysis mode in percentages.*

Figure 12. *The implemented low-cost, portable harmonic radar.*

Figure 13. *The implemented harmonic radar with a telescopic cane.*

As an example, consider the start and stop frequencies $f_{start} = 1{,}950$ MHz, $f_{stop} = 2{,}050$ MHz, $\Delta f = 1$ MHz, and $\Delta A = 10$ dB, with the results for all targets given in Table 3. The amplitude-difference threshold between the harmonic strengths is ΔA. At this setting, the system is able to finish the job within $22.24 \times 101 = 2{,}246$ ms. When we increase Δf to 10 MHz to make the system faster, the results are given in Table 4. When ΔA is 5 dB, the results are provided in Table 5. In these tables, the maximum percentages are underlined.

ST_1 is classified as semiconductor for 61% and undetermined for 39% at 10 cm as shown in Table 3. As the distance is increased, all undetermined percentages move to semiconductor. With these results, the user can make the following conclusions:

- ST_1 has strong semiconductor characteristics, but it includes some corrosive metal parts as well.
- ST_2 is always classified as semiconductor, and the percentages for corrosive metal and undetermined cases are small at all distances. At the 50-cm distance, it is classified as not detected. Therefore, the conclusion is that ST_2 is a pure semiconductor.
- The results for ST_3 are similar to ST_1. But the results show that ST_3 has weaker corrosive metal characteristics compared to ST_1.
- The results for CMT_1 and CMT_2 show the characteristics of purely corrosive metal.
- The "both" case shows high semiconductor, corrosive metal, and undetermined percentages. As the distance is increased, the corrosive metal and undetermined percentages move toward semiconductor. This is similar to ST_1, but the user can say that the "both" condition has higher corrosive metal characteristics than the ST_1 target.

Finally, the accuracy of the harmonic comparison method is degraded by the path-loss difference and the harmonic characteristics of the targets. Therefore, an analysis mode for NLJD systems will improve the accuracy by providing full frequency response maps at different distances. The normal operational mode of the implemented system is based on the harmonic comparison method. When the system harmonic-signals appropriately, users can move to the analysis mode to analyze the characteristics of the target using the proposed algorithm. Normal operational mode and the analysis mode of the system are shown in Figure 11(a) and (b), respectively.

As illustrated in Figure 12, the implemented harmonic radar is low in cost (the estimated cost is approximately €1,800) and portable (the dimensions are 20 cm × 30 cm × 11 cm, and the weight is 1.7 kg). With this size and weight, the system is suitable for

To simulate the false alarm condition, two corrosive metal targets were constructed.

handheld applications. In the example liquid crystal display shown in Figure 12, H2 indicates the second harmonic level, and H3 indicates the third harmonic level. Figure 13 illustrates the portable harmonic radar with a 1.2-m telescopic cane to provide different standoff distances.

Conclusions

We have presented a complete design of a harmonic radar for electronic countersurveillance applications. The system has +32 dBm Tx output power and −130 dBm Rx sensitivity. The radar is able to transmit at the frequency band of 1,950 MHz–2,050 MHz and receive at the range of 3,900 MHz–6,150 MHz. The total power dissipation is approximately 11 W, excluding host processor and GUI. This power dissipation can be reduced by turning off the radar for a portion of time or reducing the Tx output power.

The detection range of the NLJD radar is more than 50 cm for semiconductor and corrosive metal targets, depending on the target characteristics. The selection of transmit frequency has an important effect on the detection sensitivity, and more than one frequency (or a range of frequencies) should be used to increase the detection performance of the harmonic radar.

We have provided a novel frequency response analysis algorithm to be used in this type of system for increasing the user's knowledge about hidden objects. The proposed algorithm is applied to various semiconductor and corrosive metal targets to show improvements in accuracy when using the proposed detection algorithm. In addition, the proposed algorithm shows good accuracy when applied to challenging targets when both semiconductor and corrosive metals are within the radar's range.

Acknowledgments

We would like to thank to Kadir Sari, Serkan Kaya, Daghan Dogan, and Isa Gundogdu for their support in manufacturing.

References

[1] G. J. Mazzaro, A. F. Martone, and D. M. McNamara, "Detection of RF electronics by multitone harmonic radar," *IEEE Trans. Aerosp.Electron. Syst.*, vol. 50, pp. 477–490, Jan. 2014.

[2] J. Kositsky, "UXO detection system by harmonic radar," SRI International, Menlo Park, CA, Tech. Rep. UX-1071, May 1999.

[3] J. Welsh and R. N. Vaughan, "Article surveillance," U.S. Patent 4 063 229, Dec. 13, 1977.

[4] B. G. Colpitts and G. Boiteau, "Harmonic radar transceiver design: Miniature tags for insect tracking," *IEEE Trans. Antennas Propag.*, vol. 52, pp. 2825–2832, Nov. 2004.

[5] D. Psychoudakis, W. Moulder, C.-C. Chen, H. Zhu, and J. L. Volakis, "A portable low-power harmonic radar system and conformal tag for insect tracking," *IEEE Antennas Wireless Propag. Lett.*, vol. 7, pp. 444–447, Aug. 2008.

[6] J. Saebboe, V. Viikari, T. Varpula, H. Seppa, S. Cheng, M. Al-Nuaimi, P. Hallbjorner, and A. Rydberg, "Harmonic automotive radar for VRU classi cation," in *Proc. Radar Conf.—Surveillance Safer World*, Oct. 2009, pp. 1–5.

[7] Information Security Associates. (January 2008.) Boomerang series non-linear junction detector data sheet. [Online]. Available: http://www.isa-technology.com/products/items/boomarang4.html

[8] R. Pavlik and V. Polacek, "The detection performance of complex cosine CWT and entropy analysis for narrowband signals," in *Proc. 11th Int Radar Symp.*, June 2010, pp. 1–4.

[9] R. Hstger, "Harmonic radar systems for near-ground in-foliage nonlinear scatterers," *IEEE Trans. Aerosp. Electron. Syst.*, vol. AES-12, no. 2, pp. 230–245, Mar. 1976.

[10] S. J. Holmes and A. B. Stephen, "Non-linear junction detector," U.S. Patent 6 897 777, Feb. 11, 2002.

[11] T. H. Jones and B. R. Barsumian, "Non-linear junction detector," U.S. Patent 6 057 765, Oct. 7, 1998.

[12] S. Gruszczynski and K. Wincza, "Analog coherent detection in application to high-sensitivity nonlinear junction detectors," in *Proc. AFRICON*, Sept. 2011, pp. 1–5.

[13] S. Group. (2011). NR-2000 multipurpose non-linear junction detector data sheet. [Online]. Available: http://www.stt-group.com/prod/self/srch/

[14] Research electronics international Q1-2004 newsletter. (2004, Mar.). [Online]. Available: http://www.research-electronics.com/downloads/

[15] A. B. Stephen, I. R. Powell, and A. D. Redman, "Non-linear junction detector," U.K. Patent G B25 051 73A, Feb. 26, 2014.

[16] I.-H. Kim, K.-S. Min, J.-H. Jeong, and S.-M. Kim, "Circularly polarized tripleband patch antenna for non-linear junction detector," in *Proc. Asia-Pacific Microwave Conf.*, Nov. 2013, pp. 140–142.

[17] B. Madhav, C. Raja, K. Kumar, R. Narsingu, and G. K. Reddy, "Circularly polarized wideband archimedean spiral antenna," *Int. J. Comput. Sci. Applicat.*, vol. 1, pp. 1–7, June 2012.

[18] V. Polacek and R. Pavlik, "The use of digital modulation signals in radar system for detection of nonlinear scatterers," in *Proc. Int. Radar Symp.*, Sept. 2011, pp. 743–747.

[19] J. Zhang, X. J. Liu, and Y. Li, "Design and implementation of nonlinear junction detection FPGA-based system," *Adv. Mater. Res. Mechatron. Mater. Process. I*, vols. 328–330, pp. 2069–2073, Sept. 2011.

[20] H. A. Augenblick, "Harmonic detection system," U.S. Patent 3 631 484, July 30 1969.

[21] N. Ida, J. H. Payer, and X. Shan, "Electromagnetic radiation effects on corrosion," in *Proc. DoD Corrosion Conf.*, Aug. 2011.

[22] N. Ida, Y. L. Menach, and J. Payer, "A nonlinear model for AC induced corrosion," *Adv. Electro-Magn.*, vol. 1, no. 1, pp. 92–96, May 2012.

[23] F. Alimenti and L. Roselli, "Theory of zero-power RFID sensors based on harmonic generation and orthogonally polarized antennas," *Prog. Electromagn. Res.*, vol. 134, pp. 337–357, 2013.

[24] M. R. McMillian, "Non-linear junction characterization," Dept. Natl. Defence, Defence Research Establishment, Ottawa, ON, Canada, Tech. Rep. TN-79-7, May 1979.

[25] I. Schnitzer, A. Rosenberg, and A. Deutsch, "Radar system and method," U.S. Patent 777 767 2B2, Aug. 17, 2010.

[26] D. M. Pozar, *Microwave and RF Design of Wireless Systems*. Hoboken, NJ: Wiley, 2000.

[27] W. C. Stone, "Electromagnetic signal attenuation in construction materials," in NIST Construction Automation Program, Building and Fire Research Laboratory, Natl. Inst. Stand. Technol., Gaithersburg, MD, Tech. Rep. 3, Oct. 1997.

[28] A. Georgiadis, H. Rogier, L. Roselli, and P. Arcioni, *Microwave and Millimeter Wave Circuits and Systems: Emerging Design, Technologies and Applications*. Hoboken, NJ: Wiley, 2012.